Chapter- 4

Morphological Analysis of TPMS Scaffolds

4.1 Introduction

According to the literature, the morphological characteristics of scaffolds include porosities, pore sizes, strut thicknesses, pore shapes, and surface area-to-volume ratio (Buchanan 2008). The biological characteristics of the scaffolds are affected in various ways by these parameters. For tissue scaffolds, high porosity is a useful property because it promotes cell migration and proliferation that further accelerates biodegradation (Karageorgiou and Kaplan 2005). The wall thickness influences the biodegradation rate and mainly depends on the design (Tormala et al. 1991, Hurrell et al. 2003, Grizzi et al. 1995). The model, which should be biomimetic to optimize cell attachment and proliferation capabilities of the 3D scaffolds (in this study, the pore shapes vary by the TPMS designs), defines the shape of pores (pore size, homogeneity, and the percentage of closed, blind-end, or open holes) (Buchanan 2008). In order to promote cell development, a high surface area per volume is preferred (Tormala et al. 1991). This also accelerates the biodegradation of the scaffolds. When other parameters stay constant, all of the aforementioned relationships exist. As a result, evaluating such features is essential. This section reports and evaluates the most pertinent morphological characteristics of the multiple porosity levels of TPMS structures used in this study. The structures which are involved in this study are selected on the basis of previous reports on the advantages of these structures and their use in tissue engineering applications as discussed in the literature sections. Additionally, the critical size of unit cells and number of unit cells in lattices are taken on the basis of the study performed in Chapter-3 on the finite number of unit cells in a lattice and finite sizes of unit cells. To study the influence of porosity type as seen in Figure 4.1, four different TPMS lattice structures including Primitive (P), Gyroid (G), Diamond (D), and IWP were designed by the technique discussed in Chapter-4, with different porosity levels. To investigate the effect of porosity level, six porosity levels 40%, 50%, 60%, 70%, 80%, and 90% were designed. All

designed porous lattice structures were made of 8 unit cells (2 × 2 × 2), each unit cell having the dimensions of 1mm x 1 mm x 1 mm.

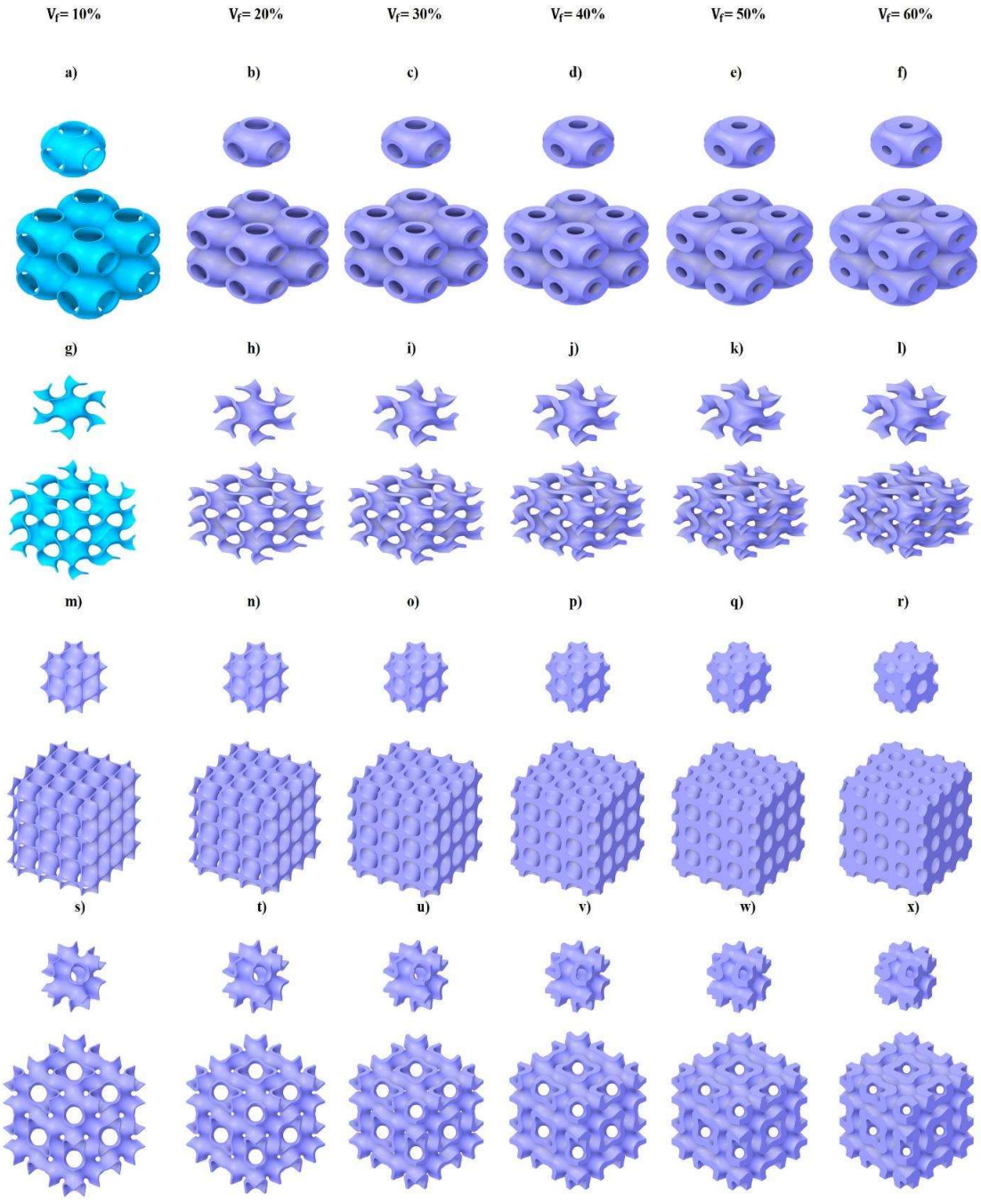

Figure 4.1: Designed porous structures with different levels of porosity and different porosity types: a-f) Primitive; g-i) Gyroid; m-r) Diamond; s-x) IWP. For each set of porosity type, top structure is unit cell of 1×1×1 mm and bottom are lattice structure which is pattern of unit cell in three coordinates having size of 2×2×2 mm. And for each set of porosity type, viewing from right to left, the level of porosity varies with 10% of intervals from 40% to 90%. (V_f indicates the volume fraction which is the opposite of porosity)

4.2 Morphological estimations

4.2.1 Porosity

The porosity of TPMS models was assessed to determine the compatibility of design for implants and was computed using the following equation.

$$\text{Porosity (\%)} = 1 - \left(\frac{V}{V_S}\right) \text{x}100 \qquad (1)$$

Where; V and V_s are volumes of solid structure and porous structure, respectively as shown in Figure 4.2.

However, for TPMS structures, porosity is highly dependent on the level constant parameter 'c' which was discussed in detail in Section 3.3.1 of Chapter 3.

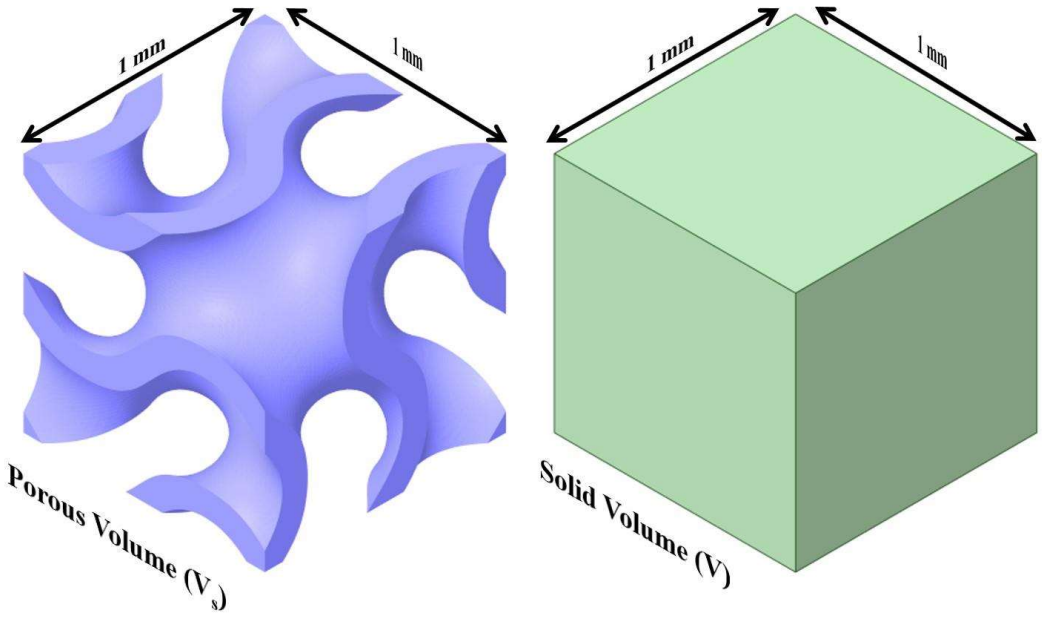

Figure 4.2: Illustration of porous volume (V_s) and solid volume (V)

4.2.2 Pore size

The pore size of a unit cell was defined by the diameter of the sphere which can be fitted in the smallest channel of the TPMS lattice structure as shown in Figure 4.3 (Vijayavenkataraman et

al. 2018). Details of the Pore size of each structure for different porosity level are listed in Table 4.1.

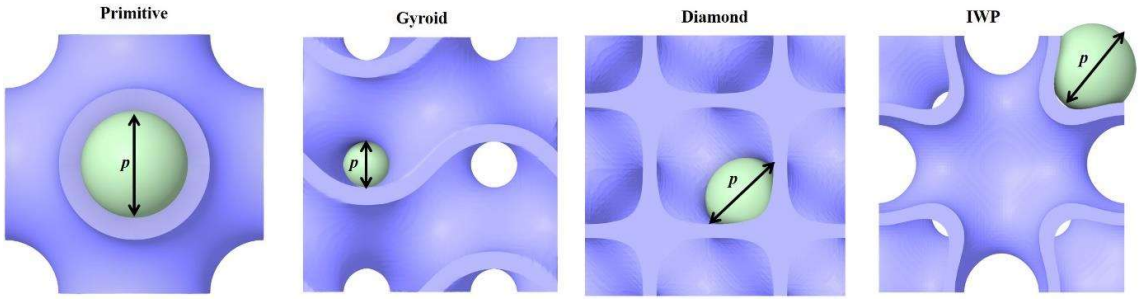

Figure 4.3: TPMS unit cells with the pore size definition in which pore size are labelled by ***p***,

Table 4.1: Estimated pore size of TPMS structures

		Pore size (*p*) (µm)			
	TPMS Structure	**P**	**G**	**D**	**IWP**
Porosity (%)	90	440	218	330	330
	80	410	180	300	310
	70	370	150	270	270
	60	330	120	240	240
	50	290	90	210	200
	40	250	60	180	160

4.2.3 Thickness

Strut thickness is an important morphological parameter for designing a porous structure since, variation in strut thickness results in a change of porosity and vice-versa. Also, strut thickness plays a major role in 3D printing methods and provides a design space in various additive manufacturing techniques. The thickness of all four TPMS structure was measured by the CAD measuring tool as shown in Figure 4.4 and thickness of all the structures is listed in Table 4.2.

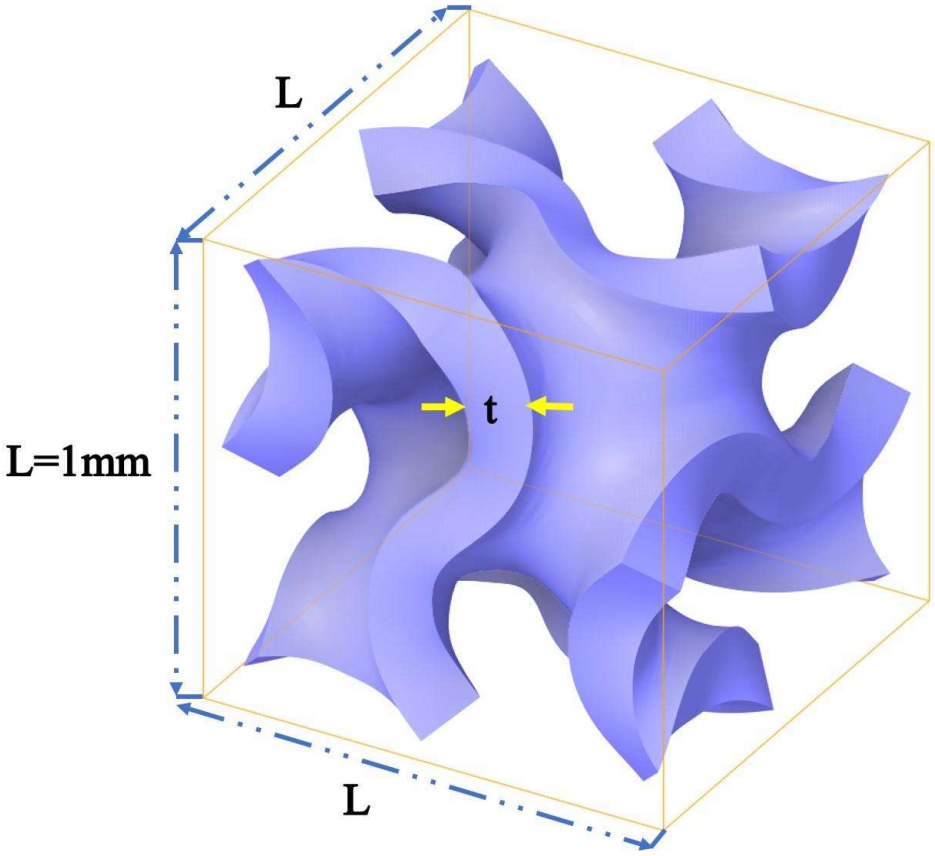

Figure 4.4: Illustration of thickness determination for TPMS structures

Table 4.2: Estimated thickness of TPMS structures

		Thickness (µm)			
	TPMS Structure	**P**	**G**	**D**	**IWP**
Porosity (%)	90	42	34	21	20
	80	85	64.4	50	50
	70	127	97	80	80
	60	170	128	110	110
	50	212	161	140	130
	40	256	193	170	150

4.2.4 Surface-Area-to-Volume ratio (SA/V_p)

Surface area to volume ratio (S/VP) is an important parameter to know the topological and biomorphic aspects when designing a scaffold with porous unit cells, it defines the total surface area per unit volume in a porous TPMS structure. Previous research on these geometrical aspects claimed that a larger surface area improves cell adhesion and bone ingrowth, as well as promotes cell proliferation metrics (Vijayavenkataraman et al. 2018). The volume and surface of each lattice cell of 2×2×2 mm were calculated by CAD measuring features. The surface area increased with the increase of porosity and, contrarily, it decreased as the thickness of cells increased and vice versa. The surface area-to-volume ratio (S/V_p) for all the structures is listed in Table 4.3.

Table 4.3: Estimated volumes and surface area of the structures and its calculated Surface-area-to-volume-ratio

TPMS Structure	Porosity (%)	Volume of structures (V_p)(mm^3)	Surface area of Structures (SA)(mm^2)	Surface-area-to-volume-ratio (SA/V_p)(mm^{-1})
Primitive (P)	90	0.7883	18.769	23.8094634
	80	1.5954	18.769	11.76444779
	70	2.3837	18.769	7.873893527
	60	3.1945	18.769	5.875410862
	50	3.9941	18.769	4.699181292
	40	4.8049	18.769	3.906220733
Gyroid (P)	90	0.84354	24.81	29.41176
	80	1.5978	24.81	15.52760045
	70	2.4066	24.81	10.30914984
	60	3.193	24.81	7.770122142

	50	3.9944	24.81	6.211195674
	40	4.7883	24.81	5.181379613
Diamond (D)	90	0.7432	68.8952	92.7007535
	80	1.5536	73.9296	47.58599382
	70	2.376	77.5056	32.62020202
	60	3.1944	79.8104	24.98447283
	50	4.0176	80.8376	20.12086818
	40	4.8408	81.8648	16.9114196
IWP	90	0.7592	59.7144	78.65437302
	80	1.5344	62.1872	40.5286757
	70	2.3624	64.2912	27.21435828
	60	3.2008	65.84	20.56985754
	50	4.0584	66.7528	16.44805835
	40	4.916	67.6656	13.76436127

From Tables 4.1, 4.2, and 4.3 it can be observed that TPMS structures allow unique tuning of their morphological parameters like porosity, pore size, thickness, and surface area, which can also tune the other properties such as mechanical and fluidic characteristics like permeability which leads to the enhanced biomechanical properties (Al-Ketan et al. 2020, O'Brien et al. 2007, Montazerian et al. 2019, Zhang et al. 2019, Santos et al. 2020). Thus, enabling them a good candidate to design bone replacement implants.

4.3 Summary

A variation in pore size and thickness was achieved by simultaneously controlling the level set constant (c) of Equations (3.3) to Equation (3.6) for D, G, IWP, and P respectively, to achieve

varying porosities of unit cells. Due to the periodic nature of TPMS in all directions, the pore sizes were the same for both D and IWP unit cells. Figure 4.5 compares the key morphological parameters between all structures in porosity and pore sizes. It was observed from the results that the pore size of P unit cells was higher in comparison to all three structures for all the porosity levels. For the increase in the porosity level, there was almost a linear increase in pore sizes in all four unit cells. Open pores having pore sizes above 100 µm were found suitable for cell integration as well as vessel regeneration (Schliephake et al. 1991, Van Blitterswijk et al. 1986). From Figure 4.5, P unit cells with porosities ranging from 40% to 90% were confirmed to have pore sizes larger than 100 µm, while G unit cells, which possessed only the unit cell having porosities in the range of 60% to 90%, showed pore size greater than 100 µm. Whereas, diamond and IWP for the porosity ranging from 40% to 90% having a pore size greater than 100 µm.

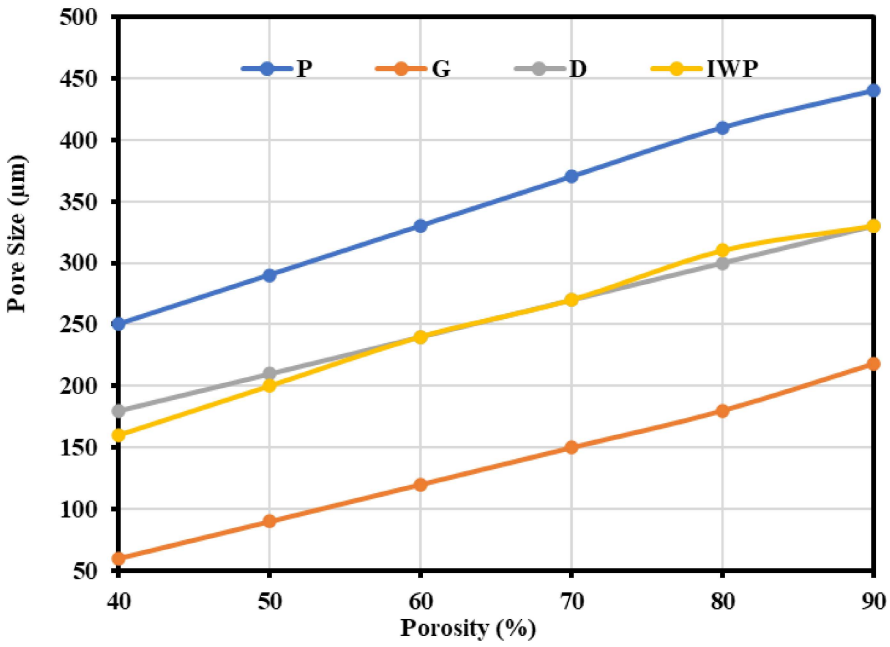

Figure 4.5: Pore sizes of porous structures with different porosity levels.

Since, strut thickness play important role in manufacturability by additive manufacturing technique. From previous report, as reported in the literature, for additive manufacturing the minimum strut thickness should be 120 µm (Mahmoud et al. 2019). Each structures of porosity 60% have strut thickness higher than 150 µm, whereas only, Primitive structures with a porosity level of 70% have strut thickness above 150 µm. Else, structures excluding those porosities mentioned above are not admissible for additive printing. Conclusively, based on the strut thickness as one parameter we have selected Primitive structures of 70 % porosity for designing patient specific scaffold as well as to demonstrate the conceptual model of implant for the treatment of large bone defects. However, for deterministic selection criteria of these structures were made on basis of mechanical and fluidic analysis which is discussed in later chapters.

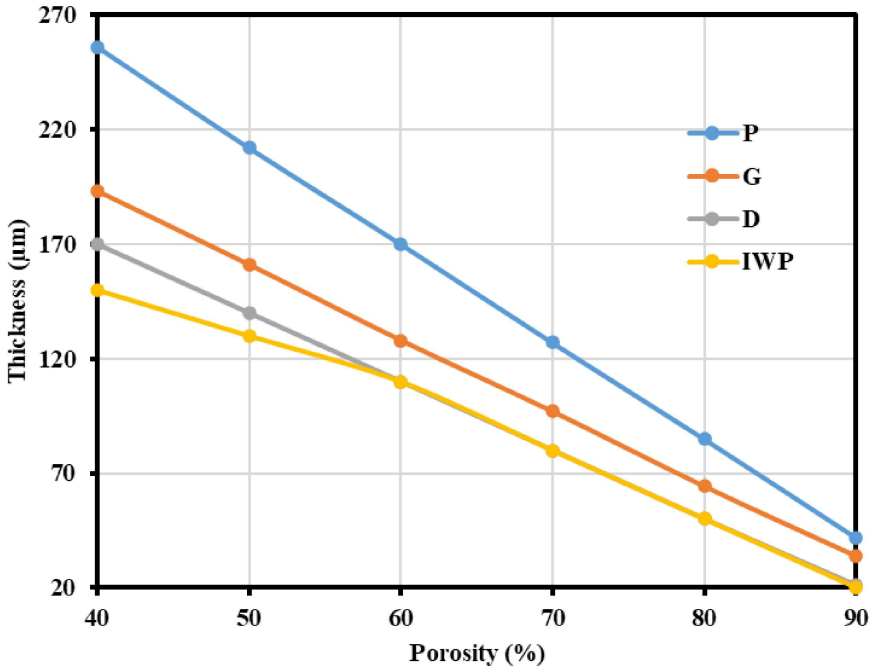

Figure 4.6: Thickness of porous structures with different porosity levels.

Surface area to volume ratio (SA/V_P) is an important parameter when designing a scaffold with porous unit cells. Previous research on these geometrical aspects claimed that a larger surface area improves cell adhesion and bone ingrowth, as well as promotes cell proliferation metrics

(Vijayavenkataraman et al. 2019). The volume and surface of each unit cell were calculated by CAD measuring features. The surface area increased with the increase of porosity and, contrarily, it decreased as the thickness of cells increased and vice versa. Figures 4.7 are the graphs for porosity versus surface to volume ratio (SA/V_P) for all four structures of varying porosity levels. From Figure 4.7 it is evident that Diamond has the highest SA/V_p among all structures for different porosity levels whereas primitive possess the lowest ratio.

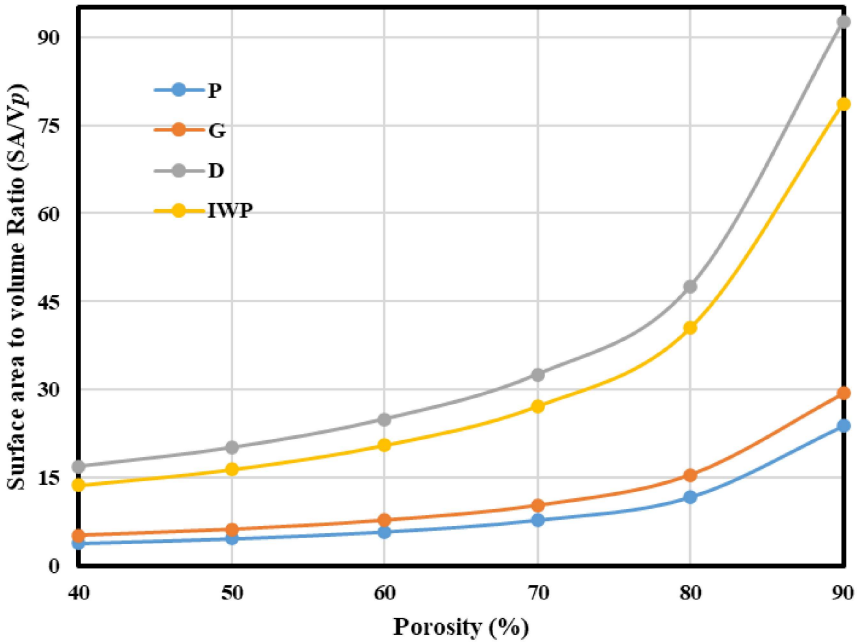

Figure 4.7: Surface area to volume ratio of porous structures with different porosity levels.

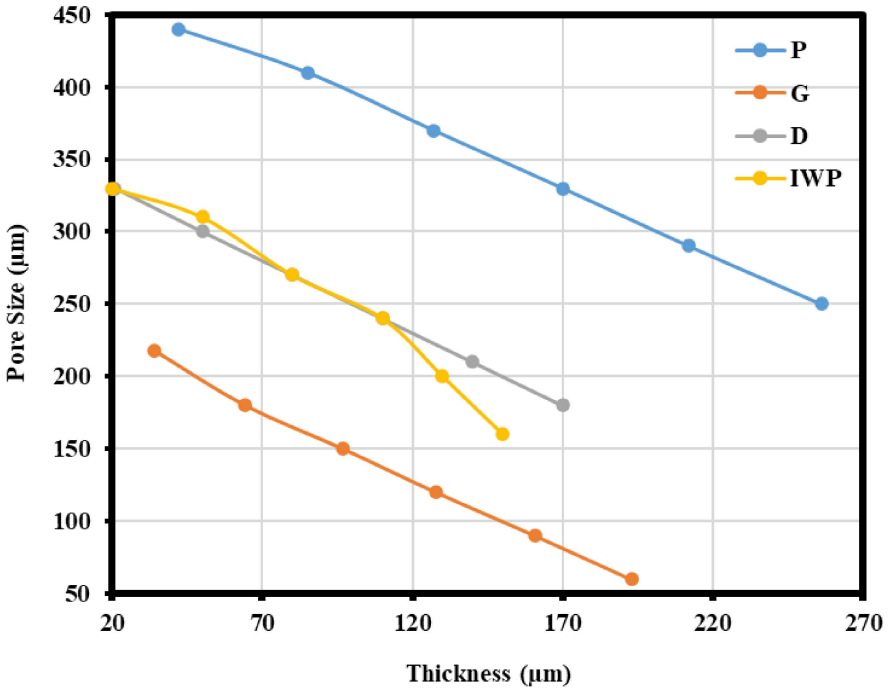

Figure 4.8: Pore sizes of structures with varying thickness levels.

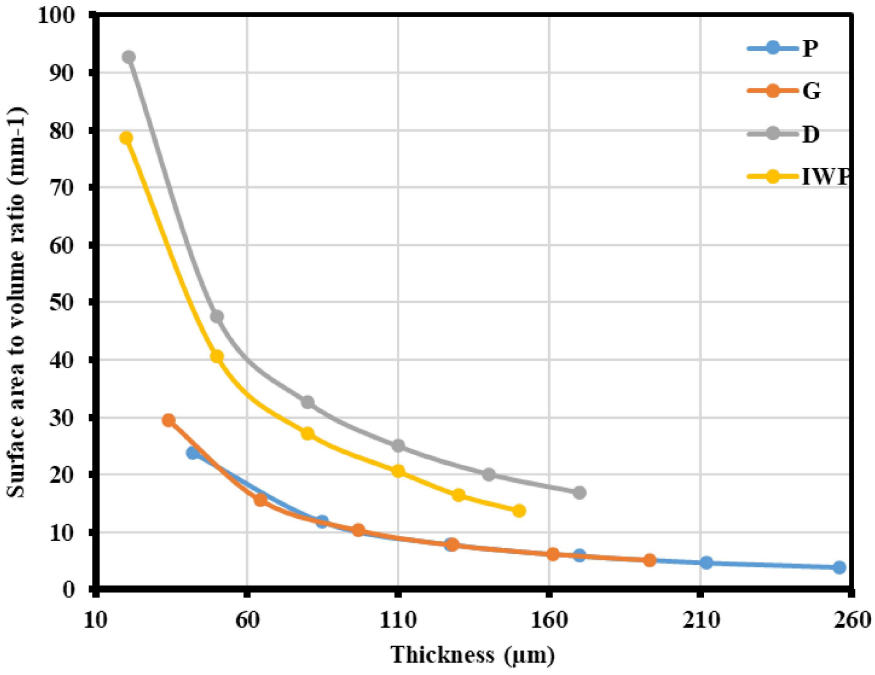

Figure 4.9: Surface area to volume ratio of structures with varying thickness levels.

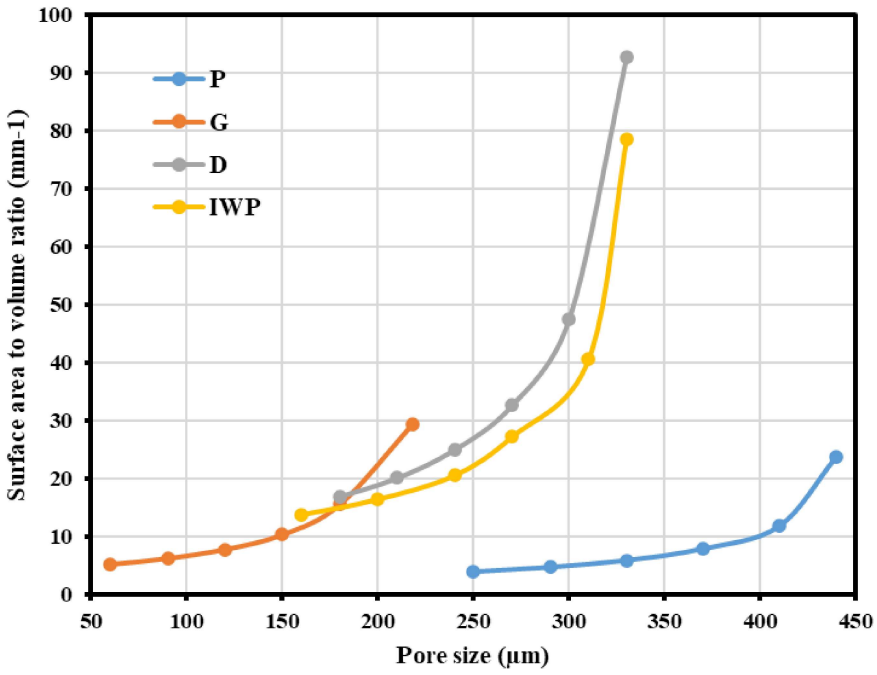

Figure 4.10: Surface area to volume ratio of porous structures with different pore sizes.

Based on the data obtained from the measurement of geometrical parameters, parameter variations were also plotted such as in Figure 4.8 Pore size Vs Thickness, in Figure 4.9 SA/V_p Vs Thickness and in Figure 4.10 SA/V_p Vs to obtain a relationship for each structure among parameters using a polynomial fit ($R^2 = 1$) between the thickness parameter, porosity of scaffolds, pore sizes and surface area to volume ratio (SA/V_p). Established Equations (4.1)–(4.24) are listed below.

For the P structure:

$$t = 0.0009X^2 - 4.3846X + 429.64 \quad (4.1)$$

$$p = -2e^{-05}X^4 + 0.005X^3 - 0.4326X^2 + 20.431X - 138.77 \quad (4.2)$$

$$p = 1e^{-09}t^5 - 9E\text{-}07t^4 + 0.0003t^3 - 0.039t^2 + 1.8043t + 415.92 \quad (4.3)$$

$$U = 4e^{-07}X^5 - 0.0001X^4 + 0.013X^3 - 0.7489X^2 + 21.367X - 237.59 \quad (4.4)$$

$$U = -2e^{-10}t^5 + 2e^{-07}t^4 - 8e^{-05}t^3 + 0.0134t^2 - 1.2594t + 57.952 \quad (4.5)$$

$$U = 1e^{-09}p^5 - 2e^{-06}p^4 + 0.0011p^3 - 0.3626p^2 + 58.342p - 3725.1 \quad (4.6)$$

For the G structure:

$$t = 5e^{-05}X^3 - 0.0077X^2 - 2.8249X + 315.22 \quad (4.7)$$

$$p = 2e^{-05}X^4 - 0.004X^3 + 0.3461X^2 - 10.145X + 123.02 \quad (4.8)$$

$$p = -6e^{-09}t^5 + 3E\text{-}06t^4 - 0.0008t^3 + 0.0833t^2 - 5.2813t + 327.01 \quad (4.9)$$

$$U = 3e^{-07}X^5 - 7e^{-05}X^4 + 0.0079X^3 - 0.4397X^2 + 12.154X - 129.14 \quad (4.10)$$

$$U = -1e^{-09}t^5 + 9e^{-07}t^4 - 0.0002t^3 + 0.0304t^2 - 2.1493t + 75.161 \quad (4.11)$$

$$U = 4e^{-08}p^4 - 1e^{-05}p^3 + 0.0019p^2 - 0.0868p + 6.0049 \quad (4.12)$$

For the D structure:

$$t = 0.0009X^2 - 3.1018X + 292.75 \quad (4.13)$$

$$p = 9e^{-16}X^2 + 3X + 60 \quad (4.14)$$

$$p = 0.0001t^2 - 1.0239t + 351.27 \quad (4.15)$$

$$U = 1e^{-06}X^5 - 0.0004X^4 + 0.0409X^3 - 2.3197X^2 + 65.224X - 711.32 \quad (4.16)$$

$$U = -6e^{-09}t^5 + 3e^{-06}t^4 - 0.0008t^3 + 0.0909t^2 - 5.5036t + 174.89 \quad (4.17)$$

$$U = 5e^{-09}p^5 - 6e^{-06}p^4 + 0.0028p^3 - 0.6362p^2 + 73.151p - 3331.7 \quad (4.18)$$

For the IWP structure:

$$t = -2e^{-06}X^5 + 0.0008X^4 - 0.1087X^3 + 6.9167X^2 - 216.1X + 2810 \quad (4.19)$$

$$p = -7e^{-06}X^5 + 0.0021X^4 - 0.2658X^3 + 16.287X^2 - 484.35X + 5730 \quad (4.20)$$

$$p = 8e^{-08}t^5 - 4E\text{-}05t^4 + 0.006t^3 - 0.4566t^2 + 14.326t + 183.41 \quad (4.21)$$

$$U = 9e^{-07}X^5 - 0.0003X^4 + 0.0297X^3 - 1.6773X^2 + 46.967X - 509.28 \quad (4.22)$$

$$U = 6e^{-07}t^4 - 0.0003t^3 + 0.0452t^2 - 3.4863t + 132.4 \quad (4.23)$$

$$U = 1e^{-08}p^5 - 2e^{-05}p^4 + 0.0072p^3 - 1.6626p^2 + 189.84p - 8533.7 \quad (4.24)$$

Where; (U) represents the surface area to volume ratio (S/V_p), (p) is the corresponding structure pore size, (t) is the strut thickness and porosity of the structure is denoted as (X) of the corresponding structure in the above equations.

These equations can be used directly to parametrize all the structural unit cells and can be directly modeled and manufactured for specific needs. These correlations may be beneficial for the characterization, as well as the manufacture, of optimized implants in osseous reconstruction to improve bone ingrowth, cell adhesion, and promote osseointegration.